Infrasound signature of the post-tropical storm Ophelia at the Central and Eastern European Infrasound Network

Tereza Šindelářová, Marine de Carlo, Csenge Czanik, Daniela Ghica, Michal Kozubek, Kateřina Podolská, Jiří Baše, Jaroslav Chum, Ulrike Mitterbauer

Journal of Atmospheric and Solar-Terrestrial Physics
June 2021, Volume 127, Pages 105603 (11p.)
https://doi.org/10.1016/j.jastp.2021.105603
https://archimer.ifremer.fr/doc/00685/79662/

Infrasound signature of the post-tropical storm Ophelia at the Central and Eastern European Infrasound Network

Šindelářová Tereza [1, *], De Carlo Marine [2, 3], Czanik Csenge [4], Ghica Daniela [5], Kozubek Michal [1], Podolská Kateřina [1], Baše Jiří [1], Chum Jaroslav [1], Mitterbauer Ulrike [6]

[1] The Czech Academy of Sciences, Institute of Atmospheric Physics, Bocni II 1401, 14100, Prague 4, Czech Republic
[2] CEA, DAM, DIF, F-91297, Arpajon, France
[3] Univ. Brest, CNRS, IRD, Ifremer, Laboratoire d'Océanographie Physique et Spatiale (LOPS), IUEM, Brest. LOPS - ZI de la Pointe du Diable - CS 10070, 29280, Plouzané, France
[4] Research Centre for Astronomy and Earth Sciences, Geodetic and Geophysical Institute, Kövesligethy Radó Seismological Observatory, Meredek u. 18., Budapest, 1112, Hungary
[5] National Institute for Earth Physics, 12 Calugareni St., PO Box MG-2, 077125, Magurele, Romania
[6] Zentralanstalt für Meteorologie und Geophysik, Hohe Warte 38, 1190, Vienna, Austria

* Corresponding author :Tereza Šindelářová, email address : tersin@ufa.cas.cz

marine.decarlo@gmail.com ; czanik@seismology.hu ; daniela_ghica@yahoo.com ; kozubek.michal@ufa.cas.cz ; kapo@ufa.cas.cz ; jba@ufa.cas.cz ; jachu@ufa.cas.cz ; ulrike.mitterbauer@zamg.ac.at

Abstract :

The Central and Eastern European Infrasound Network (CEEIN) detects significant irregularities in microbarom arrivals between 15 and October 18, 2017. The processes driving the irregular microbarom arrivals are searched in the microbarom source region in the North Atlantic and in the stratospheric waveguide. Generation of microbaroms is simulated using ocean WAVEWATCHIII wave-action model and an updated source theory which combines the effects of both finite depth ocean and source directivity. Signal propagation in a uniform range independent atmosphere is considered. In the studied time interval, a dominant moving microbarom source occurs at the tail of the post-tropical storm Ophelia.

The storm Ophelia provides an opportunity to study the development of an intense microbarom source on the open ocean and particularly in coastal waters. Discrepancies between observations and modelling results are identified and discussed. This study shows that the state-of-the-art wave-action models are underestimated in coastal areas during storms which can pose a problem for civil security in coastal areas. The capability of the CEEIN stations to monitor microbaroms is proved. Measurement biases and uncertainties associated with the configurations of the CEEIN stations and current limitations of the processing method are discussed and improvements are suggested.

Highlights

► Unusual microbarom arrivals in central and eastern Europe on 15–18 October 2017. ► Back-azimuths were shifted by 20–40° from regular directions. ► Increase of signal amplitude was observed at the same time. ► Microbarom source and propagation was modelled. ► The storm Ophelia generated a moving dominant source of microbaroms.

Keywords : Microbaroms, Post-tropical storm, Microbarom source modelling, Microbarom propagation modelling

1 Introduction

Sound is defined as a longitudinal wave motion in an elastic environment. It occupies a wide frequency range. The range between the acoustic cut-off and the lower limit of human hearing is called infrasound. In the lower atmosphere, it corresponds to frequencies approximately from 0.0033 to 20 Hz. Between 0.1 and 0.6 Hz, worldwide infrasound signals are dominated by microbaroms, a coherent noise originating from ocean regions (Bowman et al., 2019; Campus and Christie, 2010; Willis et al., 2004). Microbaroms are generated by the non-linear interaction of ocean waves. They show an amplitude peak around 0.2 Hz, corresponding to twice the frequency of the ocean waves. A prerequisite for microbarom radiation is the existence of waves with similar frequencies travelling in an almost opposite

direction. This was first demonstrated for microseisms - analogous to microbaroms for the seismic signal - by Longuet-Higgins (1950) and Hasselmann (1963). Then, a similar development was proposed for microbaroms by Brekhovkikh et al. (1973) and Waxler and Gilbert (2006). More recently, a two-dimensional energy spectrum ocean wave model accounting for bathymetry and source directivity effect has been proposed by De Carlo et al. (2020), extending the source model developed by Brekhovskikh et al. (1973).

Around 0.2 Hz, a powerful source of microbaroms detected at European infrasound stations is located in the North Atlantic, south of Greenland (Hupe et al., 2018). The detection capability of microbaroms from the North Atlantic is further reinforced from October to March when the source becomes stronger due to stormy weather above the ocean and the downwind signal propagation occurs (Landès, 2012). Another microbarom source of higher dominant frequency (0.2-0.6 Hz) was identified in the eastern Mediterranean by Assink et al. (2014).

Maritime storms are recognized as a powerful source of microbaroms (e.g. Garcès et al., 2010; Willis et al., 2004). The microbarom source regions do not overlap with the storm centre where the highest wind speeds and ocean waves occur. For the open ocean, Hetzer et al. (2008, 2010) proposed that the microbarom source regions emerge at the periphery of the cyclone where storm-generated radial waves interact with the directional background swell. Stopa et al. (2011, 2012) proved that microbaroms originated from the wave interaction at the front and rear of the tropical cyclone as well as from interaction of the cyclone-generated waves with the background ocean swell. Thus, several microbarom source regions can exist around tropical cyclones, depending on the directions of the background ocean swell.

Microbarom recordings at an infrasound array exhibit a strong variability of signal amplitudes and back-azimuths essentially controlled by the global seasonal circulation of the stratospheric winds, by the amplitude and frequency of interacting ocean waves, and by the propagation range (Ceranna et al., 2019; Garcès et al., 2004; Le Pichon et al., 2009; Willis et al., 2004).

Between 15 and 18 October 2017, infrasound stations in central and eastern Europe recorded significant variations in the detection parameters of microbaroms. Variations in azimuth of signal arrivals and fluctuations of the amplitudes had a synchronized course over the extensive area from the centre of Europe to the Carpathian region; hence local influences at measuring sites cannot explain the observations. The present study aims to identify the cause of the observed variability of microbarom arrivals. We model the microbarom sources in the North Atlantic and we analyse conditions for signal propagation between the source

region and receiving infrasound stations in order to explain the observed event. The infrasound network and data processing method are presented in Section 2. The main characteristics of the recorded signals and model results are analysed and discussed in Sections 3 and 4, respectively.

2 Data and methods

2.1 Data

2.1.1 The Central and Eastern European Infrasound Network

The Central and Eastern European Infrasound Network (CEEIN) was established in 2018 by an agreement between the operators of national infrasound stations in Austria, Czechia, Hungary, and Romania. In 2019, the network was extended to the East as two Ukrainian stations joined the CEEIN. The main purpose of the CEEIN is to improve knowledge about infrasound in central and eastern Europe. It focuses on the identification of local infrasound sources, such as industry and mines, as well as detectability of sonic booms and microbaroms.

Main characteristics of the CEEIN stations that were in operation in October 2017 are summarized in Table 1. Fig. 1 presents the location of the stations, Fig. 2 their configurations and array responses to a planar wave at 0.1 Hz (middle column) and at 0.6 Hz (right column) (Evers, 2008 and references therein).

An optimal array for monitoring microbaroms should have an aperture smaller than the microbarom wavelength (~1.5 km) to maximize coherency between array elements. The requirement of inter-element signal coherency is particularly important for detections of quasi-monochromatic signals like microbaroms. Impulses with high signal-to noise ratio can successfully be detected also with a large aperture because their arrivals at the respective array elements can be identified unambiguously. Furthermore, signal coherency decreases under noisy conditions. Therefore, the location of the station in a wind protected surrounding is preferred; additionally the station should be equipped with an efficient wind noise filtering system (Christie and Campus, 2010; Marty, 2019).

The element distribution at BURARI is close to the optimal array layout for monitoring microbaroms. The inter-element distances at the WBCI array are 4-10 km; the array configuration allows building two nearly equilateral triangles of an aperture of about 4 km. The array aperture is more than twice larger than the wavelength of microbaroms and signal

coherency between the elements is lost. Therefore the ability of WBCI to record microbaroms is limited only to events with a high signal-to-noise ratio at the station. Due to the smaller array aperture of PVCI and PSZI, the resolution of back-azimuths and apparent velocities is worse near 0.1 Hz; whereas the maximum energy of microbaroms is expected around 0.2 Hz (e.g. Campus and Christie, 2010). The CEEIN stations, excluding WBCI, are thus eligible for monitoring microbaroms.

The CEEIN stations are equipped with microbarometers designed by various manufacturers. The response of the differential sensors at PVCI is flat in the 0.02-4 Hz band. Broadband sensors are installed at PSZI (nominal bandwidth of 0.01-27 Hz), BURARI, and IPLOR (flat response in the 0.1-200 Hz band at both stations). The microbarometers at WBCI measure absolute pressure in the range of 620-1100 hPa. The manufacturer guarantees high performance of the sensors between 0.001-10 Hz. The 0.1-0.6 Hz band analysed in the present study falls into the optimum performance range of all types of sensors installed at the CEEIN stations.

At PSZI, the 32 air-inlets wind noise reducing system (WNRS) is composed of 4 branches of flexible hoses divided into 8 branches equipped with crepine, with a 18-metre wingspan. The WNRS was designed by CEA (Commissariat à l'énergie atomique et aux énergies alternatives, France). The PSZI site is covered with a temperate mixed forest with relatively dense undergrowth that helps to further reduce environmental noise. At BURARI, the wind noise reduction systems consist of four porous hoses of 15 m length connected to each of the microbarometers. The station is located in a deforested mountain area at altitudes about 1000 m a.s.l. Thus, the observations can be to a higher extent disturbed by wind noise. At IPLOR, wind noise reduction system consisted of rosette pipe arrays in October 2017. The sensors are protected from wind noise also by the surrounding forest. At PVCI and at WBCI, the sensors are placed in closed boxes. PVCI sensors are distributed on a grassy plot of the observatory. This makes PVCI sensitive to wind noise. Indeed, under usual conditions microbaroms are only detected at wind speeds up to 2 $m \cdot s^{-1}$.

2.1.2 Infrasound detections with PMCC

We analyse infrasound data measured by CEEIN stations from 1 to 31 October 2017 in the frequency range of 0.1-0.6 Hz (Šindelářová et al., 2020). This band covers the frequency range in which microbarom detections are mostly reported (see Section 1). The data are processed using the Progressive Multi-Channel Correlation (PMCC) detection algorithm (Brachet et al., 2010; Cansi, 1995; Cansi and Le Pichon, 2008; Le Pichon and Cansi, 2003).

Guidelines on the time and frequency scalings in infrasound detection algorithms, applicable also for PMCC, can be found in Garcès (2013).

As can be noticed in Table 1 and in Fig. 2, the CEEIN arrays are of different apertures and of different numbers of elements. Thus, data processing requires a specific setting of PMCC configuration optimized for each of the arrays. The PMCC configurations used for routine data processing (Table 2) are suitable for monitoring microbaroms (except WBCI, see explanation in Sect. 2.1.1).

The frequency bands for detections are logarithmically scaled; the length of detection windows is tailored to the frequency range of a band (Garcès, 2013). Detection is only accepted below the consistency threshold given in Table 2 (Brachet et al., 2010). The overlap of the adjacent detection windows is given in percent of the window length. The azimuth resolution to aggregate pixels into detection (family) depends on the array aperture (Szuberla et al., 2004). Larger azimuth tolerance results in more smoothed detections in terms of back-azimuths variability and enables easier tracking of large-scale back-azimuth changes. On the other hand, small scale fluctuations can be lost.

From the resulting detection bulletins, families falling into the 0.1-0.6 Hz band and the back-azimuth range of 210-360° were considered for the analysis of the Ophelia event.

2.1.3. Tracking of the storm Ophelia

The location of the storm Ophelia is obtained from the revised Atlantic hurricane database HURDAT2 (Landsea and Franklin, 2013). The analysis of the event is adopted from the hurricane Ophelia report elaborated by the NOAA National Hurricane Center (Stewart, 2018). Ophelia tracking is shown in Fig. 1 and in Fig. 4. Table 3 sums up the information about Ophelia and back-azimuth and distance from the CEEIN stations to the storm centre.

Processes leading to the later formation of the tropical storm Ophelia were reported above the subtropical North Atlantic already at the beginning of October 2017. On 3 October, a broad surface low pressure system formed west of the north-western Azores (Stewart, 2018). On 9 October 2017, the tropical storm Ophelia formed in the Central Atlantic (around 30°N, 40°W). It became a hurricane on 11 October at 18:00 UTC. The hurricane Ophelia moved north-east towards Europe on 12 October. During its peak phase on 14 October, Ophelia reached an intensity of a category 3 hurricane with a central pressure of 959 hPa. Between 15 October, 00:00 UTC and 16 October, 00:00 UTC, Ophelia underwent a transition from a tropical cyclone to an extratropical one. The post-tropical cyclone Ophelia steadily weakened as it travelled to the north and northeast along the western coast of Europe at a

forward speed of around 15 m·s^{-1}. The radius of maximum wind velocity was relatively small, ranging between 74 and 83 km (Stewart, 2018). Ophelia made its first landfall at the coast of the British Isles on 16 October around 11:00 UTC, followed by further landfalls on the British Isles through 16:45 UTC and at 23:45 UTC. On 17 October, Ophelia left British Islands and headed towards south-west Norway where it made its final landfall at 17:30 UTC. The storm dissipated over southern Norway on 18 October around 00:00 UTC. Wind speeds reported on the British Isles reached up to 40 m·s^{-1}, a wind gust of 53 m·s^{-1} was recorded on 16 October at 10:30 UTC. Maximum wave heights of 18-26 m were reported along the south-eastern, southern, and south-western coastal areas of Ireland (Stewart, 2018).

2.2 Microbarom modelling method

2.2.1 Source modelling

Microbaroms are generated by almost opposing ocean wave interactions (Posmentier, 1967; Brekhovskikh et al., 1973; Waxler et Gilbert, 2006; De Carlo et al., 2020). These interactions can be represented by the Hasselman's integral: $H(f) = \int_0^{2\pi} E(f,\theta)E(f,\theta+\pi)d\theta$, where $E(f,\theta)$ is the directional spectrum of wave energy, and $E(f,\theta+\pi)$ the directional spectrum in the opposite direction.

Following De Carlo et al. (2020), microbarom pressure spectrum $F_{p2}(f_s,\Phi_2)$ integrated for all elevation angles θ_a at the surface generation gives

$$F_{p2}(f_s,\Phi_2) = \frac{2\pi^2\rho_a^2 g^2}{\alpha_a^2}\, 2^3 f^3\, H(f) \int_0^{90} \sin\theta_a \cos\theta_a\, |R_a|^2 d\theta_a \quad (1)$$

where $\theta_a, \rho_a, \alpha_a, g, f_s$ are respectively the elevation angle in the atmosphere, the air density, the sound speed in the air, the gravity constant, and the frequency of the microbaroms signal (twice the frequency of ocean waves f). The factor R_a is defined in equation (41) of De Carlo et al. (2020) and corresponds to the velocity potentials' ratio between ocean and atmosphere. The Hasselmann integral used for source modelling is obtained from the second order equivalent surface pressure due to ocean wave interaction as presented in Ardhuin et al. (2011). This equivalent surface pressure is computed by the Institut Français de Recherche pour l'Exploitation de la MER (IFREMER) from ocean wave-action model outputs using the WAVEWATCHIII® code (The WAVEWATCHIII® Development Group, 2016) with the parametrization described in Rascle and Ardhuin (2013) and stored in 'p2l' files. These files are available for 22 frequency bands between f = 0.04 Hz and f = 0.3 Hz, with a three-hour time step and a grid resolution of 0.5° both in latitude and longitude. Therefore, the

microbarom model used shows the same spatial and temporal resolutions and ranges from f_s= 0.08 Hz to f_s= 0.6 Hz.

2.2.2 Propagation

To obtain a modelled signal comparable with the observations at CEEIN stations, the infrasound propagation has to be taken into account. A straight-forward way to do so is to use the semi-empirical attenuation law given by Le Pichon et al. (2012) derived from parabolic equation simulations, assuming uniform atmospheric conditions along the propagation path. This attenuation law accounts for the frequency, the distance between the source and the station and the effective sound speed ratio in the propagation direction. The effective sound speed ratio $v_{eff_{ratio}}$ is the ratio between the stratospheric sound speed c_{strato} plus the along-path wind $\boldsymbol{u_{strato}}$ in the propagation direction $\boldsymbol{x}$ and the sound speed at ground level c_0.

$$v_{eff_{ratio}} = \frac{c_{strato} + \boldsymbol{u_{strato}} \cdot \boldsymbol{x}}{c_0} \qquad (2)$$

As this attenuation law considers a horizontally uniform atmosphere, the profile used to compute $v_{eff_{ratio}}$ is chosen to be representative of the atmosphere along the propagation. Two main profiles are identified. First, the one at the respective grid point represents the propagation conditions at the potential source, indicating if the acoustic energy can propagate towards the receivers through a stratospheric waveguide. Second, the profile at the station indicates if the propagation conditions allow the detection of the signal far off the source. In this study, the atmospheric conditions are quite extreme at the source, and thus they might not be representative of the propagation path. Therefore, the profiles at the stations are extracted from the ECMWF (European Centre for Medium-Range Weather Forecasts) ERA5 reanalysis product distributed by Copernicus Climate Change Service (C3S) Climate Data Store (CDS) (https://cds.climate.copernicus. eu/cdsapp#!/home).

2.2.3 Directional spectrum at the station and quantities of interest

In order to compare model results with the observations, the modelled directional pressure spectrum is computed at the station. To do so, for each cell *i* of the source model, the directional pressure spectrum $F_{p2,i}(f_s, \Phi_2)$ at the source is multiplied by the square of the propagation attenuation factor $Att_i(f_s)^2$ between the cell *i* and the station, and by the area of the cell point dS_i. Then, the resulting values are summed by azimuth – i.e. all cells intersecting with the azimuthal band (of 1°) φ are summed – and the modelled directional pressure spectrum at the station $F_{p2-sta}(\varphi, f_s)$ finally writes:

$$F_{p2-sta}(\varphi, f_s) = \sum_{i|\varphi_i=\varphi} F_{p2,i}(f_s, \Phi_2) * Att_i(f_s)^2 * dS_i \quad (3)$$

From this directional pressure spectrum, two quantities of interest are obtained at each station: the amplitude maximum and its corresponding azimuth calculated for each frequency band and time step. Therefore, for each time step, there are 22 amplitudes and dominant azimuths corresponding to the frequency bands; all these values were kept in order to account for all frequency bands similarly to PMCC processing. The modelled amplitude corresponds to the square root of the maximum – along the azimuth – of $F_{p2-sta}(\varphi, f_s)$. To compare observed and modelled amplitudes, both are normalized by their mean background value before and after the event, i.e. the amplitudes are divided by the average of the background amplitude. All ocean cells being considered in the model, the modelled microbarom amplitude corresponds to the background microbarom ambient noise during calm period. Therefore, the background amplitude is here taken as the amplitude of the calmer period from 1 to 10 October and from 20 to 31 October.

3 Results

3.1 Microbarom detections by CEEIN

Microbarom arrivals at CEEIN stations in October 2017 are shown in Fig. 3. From 1 to 15 October, the stations mostly record microbaroms from the back-azimuths of 290° to 330°. The back-azimuths are consistent with directions from the North Atlantic recorded by the CEEIN stations in winter (Bondar et al., 2019; Ghica et al., 2019; Šindelářová et al., 2016). On 7 October, the stations PSZI and BURARI transiently record microbaroms from the south-west. The back-azimuths of 230-260° at PSZI and 210-240° at BURARI point towards subtropical North Atlantic regions where the cyclone Ophelia is forming (Stewart, 2018).

Between 15 and 16 October, microbarom back-azimuths shift by 20-40° from north-west to west. The event can be observed simultaneously at PVCI, PSZI, and BURARI and a similar change in back-azimuth (in the order of this shift) is also indicated at the other stations despite temporarily missing data. Around 06:00 UTC on 16 October, microbaroms arrive from 265-290°. From 16 to17 October, microbarom arrivals gradually return to the usual north-west directions.

The changes of back-azimuths are accompanied with fluctuations of signal amplitudes. Maximum microbarom amplitudes of October 2017 can be recognized at all CEEIN stations on 16 and 17 October. At PVCI, two amplitude peaks of 0.07 Pa and 0.05 Pa

are observed on 16 October at 17:40 UTC and on 17 October at 18:00 UTC, respectively. The decrease of the amplitude below 0.03 Pa on 17 October between 09:40 and 14:50 UTC is accompanied with signal arrivals from a wide azimuth range of 40°. For comparison, the azimuth extent was less than 15° on 16 October at 17:40 UTC.

At the large aperture array WBCI, microbarom detections intermit on 17 October at 08:30 UTC. The likely reason is a decreasing signal-to-noise ratio at WBCI (see Sect. 2.1.1); the microbarom amplitude at the closest array PVCI decreases at the same time.

3.2 Signal propagation in the stratospheric waveguide

We examine whether the observed back-azimuth shift can be explained by influences along the signal propagation path. The signals propagate downwind in the stratospheric waveguide (Ceranna et al., 2019), along a propagation range of 2000 km. The propagation path may be affected by transversal wind effect from the ground to the stratopause region. We apply the method developed by Blixt et al. (2019) to estimate the average velocity of cross-winds that would cause the observed back-azimuth deviations. The average velocity of cross-winds along the signal propagation path, W is estimated as:

$$W = -v \tan(\delta) \quad , \qquad (4)$$

where v is the signal celerity and δ is the azimuth deviation. We assume a celerity range of stratospheric arrivals of 260-310 $m \cdot s^{-1}$ (Blixt et al., 2019 and references therein). According to Eq.4, back-azimuth deviation of 40° would be caused by an increase of mean cross-wind speed up to unrealistic values of ~250 $m \cdot s^{-1}$.

The stratospheric wind and temperature fields derived from ERA5 do not show major changes in their dynamics from 15 to 18 October that would influence signal propagation in the stratospheric waveguide in the way that would lead to the observed variability in azimuths of signal arrivals. Wind speed in the altitude range of the stratospheric waveguide does not exceed 80 $m \cdot s^{-1}$ above the eastern North Atlantic and above Europe from 15 to18 October; maxima occur at the altitude of the polar jet stream. Thus, the observed change of the back-azimuths cannot be explained by propagation effects only.

3.3 Modelling of the microbarom source region and comparison of the observations with the model predictions

From 15 to 17 October, the post tropical cyclone Ophelia is travelling to the north and north-east along the western coast of Europe (Table 3). According to Hetzer et al. (2008, 2010) and Stopa et al. (2011, 2012), microbarom sources develop at the periphery of a

cyclone rather than at its centre. The used model (De Carlo et al., 2020) predicts the formation of a large intense microbarom source at the tail of the Ophelia storm. This source dominates in the North Atlantic, particularly after 03:00 UTC on 16 October (Fig.4).

Along with locating the microbarom source regions in the ocean, the model provides predictions of signal back-azimuths and amplitudes at a station after its propagation in a stratified range-independent atmosphere (see Sect. 2.2). In order to investigate whether the observed variability in microbarom arrivals originates from the transient source related to the storm Ophelia we compare the observed microbarom arrivals with model predictions of signal arrivals at the stations BURARI, PVCI, and PSZI.

Standard conditions occur in the North Atlantic with a quite large and steady microbarom source before 15 October; the observations are consistent with the model predictions.

On 15 October in the first half of day, the model expects microbarom arrivals from multiple sources (Fig.5). Apart from the usually observed back-azimuths around 315°, a new source emerges with bearings of 260-270°. The new source is related to the storm Ophelia. The CEEIN stations record arrivals from the north-west source on 15 October; Ophelia as a source of microbaroms dominates the observations from16 to 17 October until it dissipates over southern Norway. The observed microbarom back-azimuths correspond to the predicted arrivals from the Ophelia-generated microbarom source with accuracy better than 10° from 16 October, 06:00 UTC to 18 October, 00:00 UTC. A higher variability of the predicted back-azimuths on 17 October occurs in the time interval when the modelled Ophelia-generated microbarom source weakens and disappears during the storm passage over the British Isles (an explanation is discussed in Section 4). Later after 15:00 UTC, a large source starts to develop in the North Sea, generated by the storm Ophelia. The source extends from the north of the British Isles to the south of Scandinavia. As a consequence, microbarom arrivals from a wide azimuth range of 300-320° are expected at the CEEIN stations on 17 October from 15:00 to 22:00 UTC.

A discrepancy between the modelled and observed back-azimuths occurs on 15 October. The model predicts a sudden change of the back azimuth from 315° to 270°, while the CEEIN stations observe a smooth transition of the back-azimuth from 15 October, 21:00 UTC to 16 October, 06:00 UTC.

The observed and modelled microbarom amplitudes match at the beginning of the Ophelia event on 15 October and on 16 October until about 12:00 UTC. A significant discrepancy between the modelled and observed amplitudes develops from the noon of 16

October; the modelled amplitude starts to decrease and in contrast the observed microbarom amplitude increases rapidly. The modelled amplitudes approximate the observed values again at the end of the day on 18 October after Ophelia made its final landfall and dissipated above Norway (Fig. 5).

4 Discussion

As mentioned in Section 3.3, large discrepancies between the modelled and observed microbarom amplitudes occur from 16 to 17 October. Ophelia approaches the west coast of Ireland on 16 October, where it makes a series of landfalls between 11:00 and 16:45 UTC (Stewart, 2018). Another landfall is reported from the north-west coast of Scotland at 23:45 UTC. The maximum radius of 26 $m \cdot s^{-1}$ winds is over 200 km on 16 October. Wind speed of 18 $m \cdot s^{-1}$ is reported at the maximum radius of about 450 km (Landsea and Franklin, 2013). Thus, the tail of the storm moves, at least partly above coastal waters. By that time, maximum amplitudes of microbaroms are observed at the CEEIN stations. In contrast, the modelled signal amplitudes decrease. It can be seen from Fig. 4 that the modelled Ophelia-generated microbarom source weakens and disappears from 16 October, 15:00 UTC to 17 October, 12:00 UTC. The complex bathymetry near coasts leads to a decreased performance of the WAVEWATCHIII® model; moreover the model tends to underestimate the significant wave height under severe weather conditions (Mentaschi et al., 2015). As a consequence, the microbarom model fails to retrieve the amplitude variation of the infrasound signal. Based on these comparisons, one could consider using microbarom detections from extreme events to enhance the wave model in coastal regions. While the authors are not optimistic in such a perspective per se - in average, only 1.6% of the total microbarom flux is emitted in coastal regions - they believe a synergy with other remote sensing methods such as satellite imageries or microseisms detections can help improve the model capacity in term of directional spectrum near the coast.

The decrease of the observed signal amplitude is evident on 17 October between 09:40 and 14:50 UTC, particularly at PVCI. At the same time, spread of microbarom back-azimuths occurs at the station. It leads to an assumption that the dominant microbarom source fades out. The travel time needed for the signal propagation from the anticipated source near the British Isles to PVCI in the stratospheric wave guide is 60-90 min. Taking into account the approximate position of the storm centre at 08:00-14:00 UTC (Table 3) and the radius of 18 $m \cdot s^{-1}$ winds (450 km) (Landsea and Franklin, 2013), we assume that the Ophelia-generated microbarom source disappears as the tail of the storm moves over Scotland.

Another discrepancy between the model and the observations occurs in azimuths of microbarom arrivals between 15 October, 21:00 UTC and 16 October, 06:00 UTC. The model predicts microbarom arrivals from multiple sources followed by a sudden change of the back-azimuth, whereas the PMCC detection bulletins at the CEEIN stations show a smooth transition of microbarom back-azimuths from north-west to west. The smooth back-azimuth transition is a data processing artefact. The data processing includes detecting the dominant source in a given time-frequency window (obtaining a detection pixel) and gathering detection pixels in families. The existence of a single dominant source in a given time-frequency window is presumed. When multiple sources of similar amplitudes are in competition, PMCC struggles to separate them. Applying high-resolution beamforming technique would allow distinguishing the signals from multiple active source regions (e.g. den Ouden et al., 2020).

The consideration of a horizontally homogenous atmosphere for signal propagation modelling is a strong assumption. However in this study, the stratospheric conditions and the strength of the source during the investigated period (see Fig. 4) justify it. Furthermore, the results are accurate enough for the purposes of this study. For analyses where further propagation accuracy is required – with more precise detections or lesser sources – one could recommend modifying the attenuation law using eq (17) of Tailpied (2016) in order to consider a range-dependent atmosphere. It should be noted that this increases the calculation time significantly.

Another drawback of the considered attenuation law relates to its associated uncertainty that generates amplitude offset at the station after the source summation. Therefore, the normalization by the background noise is necessary in this study. Further refinements in propagation and amplitude attenuation might enable to compare observed and modelled amplitudes without normalisation, which would allow focusing on possible amplitude offsets in source modelling.

The CEEIN stations are able to efficiently monitor microbaroms. However, modifications of the array layouts can still improve the detection capability of the CEEIN. The modifications can be recommended particularly at the stations PSZI and PVCI. Inter-element distances should be slightly increased to ensure a good resolution of the estimated arrival parameters also near 0.1 Hz. The array elements should be distributed homogenously in terms of inter-element distances and azimuths (Marty, 2019). Moreover, number of array elements should be increased at PVCI to comply with the International Monitoring System of the Comprehensive Nuclear-Test-Ban Treaty Organisation (IMS) requirement of at least four

elements in an array (Marty, 2019) and an upgrade of the WNRS at the station is advisable as well. The station WBCI is primarily intended for monitoring of low frequency infrasound near the acoustic cut-off (~0.0033 Hz) and for monitoring of gravity waves, therefore the array is built with large inter-element distances. Low inter-element signal coherency is expected at very large aperture arrays compared to the wavelength of the signal of interest and classical detection algorithms based on search of the coherent signals over the array elements are limited (Green, 2015). Application of other detection techniques can be recommended for such arrays. Power based detection techniques (Gibbons, 2008) or estimation of the signal parameters using the inversion of arrival times (Husebye, 1969) can provide more robust results.

5 Conclusions

Significant variations in back-azimuths and amplitudes of microbarom arrivals are observed in central and eastern Europe between 15 and 18 October 2017. The anomalous microbarom arrivals are related **to** the post-tropical storm Ophelia that passed along the western coast of Europe from 15 to 17 October. The modelling of microbarom sources in the North Atlantic reveals a dominant microbarom source at the tail of the storm. The analysis of signal propagation in a stratified range independent atmosphere proves that the CEEIN stations observe microbaroms from the Ophelia-generated source.

Ophelia is one of the rare major hurricanes that hit the eastern North Atlantic and - at the extra-tropical storm stage – the west of Europe. Ophelia track passes over the British Isles. The event thus provides, besides observations of a microbarom source related to a maritime storm**,** an opportunity to study an intense microbarom source in coastal waters. The observations at the CEEIN stations imply that coastal waters can transiently be an efficient source of microbaroms. The modelled microbarom amplitudes are significantly underestimated when the dominant microbarom source approaches the coast. The underestimation of the modelled microbarom amplitudes follows from the underestimation of waves - in particular, opposing waves in coastal regions - by the sea state model. Thus, we advise to increase the performance of sea state models in coastal regions. A good performance of the sea state models in coastal areas under severe weather conditions can be of interest e.g. for civil security applications and can gain even more importance in the future in the context of predicted increasing ocean level due to climate change (e.g. https://climate.nasa.gov/vital-signs/sea-level/ and https://sealevel.nasa.gov/).

The CEEIN stations in their current layouts and detection algorithm settings are able to efficiently monitor microbaroms, as proved by the present study. At a distance of the order of thousands of kilometres, the CEEIN can contribute to monitoring of severe weather above eastern parts of the North Atlantic and it is able to capture standard conditions in the microbarom source region in the Northern Atlantic as well. Thanks to their ubiquity, microbaroms are regarded a promising phenomenon for probing the middle atmosphere in the future (Blanc et al., 2018). For monitoring purposes, a dense coverage of regional infrasound stations such as the CEEIN network supporting the global IMS network is essential to improve detection capability in the eastern European region. Optimization of the CEEIN array layouts and integration of alternative data processing techniques are proposed to improve the CEEIN performance for those purposes.

Acknowledgements

The work was supported by the Czech Academy of Sciences [mobility project MTA-19-01]; the Czech Science Foundation [grant 18-01969S].

The Hungarian infrasound studies are supported by the Hungarian National Research, Development and Innovation Fund [K128152].

The DTK-GPMCC software was kindly provided by Commissariat à l'énergie atomique et aux énergies alternatives, Centre DAM-Île-de-France, Département Analyse, Surveillance, Environnement, Bruyères-le-Châtel, F91297 Arpajon, France.

The authors thank Alexis Le Pichon and Julien Vergoz for advanced training to process infrasound data and helpful discussions during the completion of this study and Péter Mónus for the technical support for the PSZI array.

Data availability

The modelled second order equivalent surface pressure due to ocean wave interaction is available at ftp://ftp.ifremer.fr/ifremer/ww3/HINDCAST/SISMO/GLOBAL05_2017_REF102040/WW3-GLOB-30M_201710_p2l.nc

The CEEIN infrasound data are available in the repository 4TU.Centre for Research Data (Šindelářová et al., 2020).

References

Ardhuin, F., Stutzmann, E., Schimmel, M., Mangeney, A., 2011. Ocean wave sources of seismic noise. J. Geophys. Res. 116, C09004. doi: 10.1029/2011JC006952

Assink, J., D., Waxler, R., Smets, P., Evers, L.G., 2014. Bidirectional infrasonic ducts associated with sudden stratospheric warming events. J. Geophys. Res. Atmos. 119, 1140-1153. doi: 10.1002/2013JD021062

Blanc E., Ceranna L., Hauchecorne A., Charlton-Perez A. J., Marchetti E., Evers L. G., Kvaerna T., Lastovicka J., Eliasson L., Crosby N. B., Blanc-Benon P. , Le Pichon, A., Brachet, N., Pilger, C., Keckhut, P., Assink, J.D., Smets, P.S.M., Lee, C.F., Kero, J., Sindelarova, T., Kämpfer, N., Rüfenacht, R., Farges, T., Millet, C., Näsholm, S.P., Gibbons, S.J., Espy, P.J., Hibbins, R.E., Heinrich, P., Ripepe, M., Khaykin,S., Mze, N., Chum, J., 2018. Toward an improved representation of middle atmospheric dynamics thanks to the ARISE project. Surv. Geophys., 39, 171-225. https://doi.org/10.1007/s10712-017-9444-0

Blixt, E.M., Nasholm, S.P., Gibbons, S.J., Evers, L.G., Charlton-Perez, A.J., Orsolini, Y.J., Kvaerna, T., 2019. Estimating tropospheric and stratospheric winds using infrasound from explosions. J. Acoust. Soc Am. 146:2, 973-982. doi: 10.1121/1.5120183

Bondar, I., Czanik, C., Czecze, B., Kalmár, D., Kiszely, M., Monus, P., Sule, B., 2019. Hungarian Seismo-Acoustic Bulletin 2017-2018. http://www.infrasound.hu/index.php/en/hungarian-seismo-acoustic-bulletin (accessed 25 February 2020)

Bowman, D., Lees, J., Cutts, J., Komjathy, A., Young, E., Seiffert, K., Boslough, M., Arrowsmith, S., 2019. Geoacoustic Observations on Drifting Bolloon-Borne Sensors, in: Le Pichon, A., Blanc, E., Hauchecorn, A. (Eds.), Infrasound Monitoring for Atmospheric Studies. Challenges in Middle Atmosphere Dynamics and Societal Benefits. Springer Nature Switzerland AG, pp. 471–482. doi:10.1007/978-3-319-75140-5_4

Brachet, N., Brown, D., Le Bras R., Cansi, Y., Mialle, P., Coyne, J., 2010. Monitoring the Earth's Atmosphere with the Global IMS Infrasound Network. In: Le Pichon, A., Blanc, E., Hauchecorne A. (Eds.), Infrasound Monitoring for Atmospheric Studies. Springer Science+Business Media B.V., 77-118. Doi: 10.1007/978-1-4020-9508-5_3

Brekhovskikh, L. M., Goncharov, V. V., Kurtepov, V. M., Naugolnykh, K. A., 1973. The radiation of infrasound into the atmosphere by surface waves in the ocean. Izv. Atmos. Ocean. Phys. 9, 899–907. (In the English translation, 511–515.)

Campus, P., Christie, D.R., 2010. Worldwide Observations of Infrasonic Waves. In: Le Pichon, A., Blanc, E., Hauchecorne A. (Eds.), Infrasound Monitoring for Atmospheric Studies. Springer Science+Business Media B.V., 185234-118. Doi: 10.1007/978-1-4020-9508-5_6

Cansi, Y., 1995. An automatic seismic event processing for detection and location: The P.M.C.C. method. Geophys. Res. Lett. 22, 1021-1024. doi: 10.1029/95GL00468

Cansi Y., Le Pichon A., 2008. Infrasound Event Detection Using the Progressive Multi-Channel Correlation Algorithm. In: Havelock D., Kuwano S., Vorländer M. (Eds.) Handbook of Signal Processing in Acoustics. Springer, New York, NY. https://doi.org/10.1007/978-0-387-30441-0_77

Ceranna, L., Matoza, R., Hupe, P., Le Pichon, A., Landès, M., 2019. Systematic Array Processing of a Decade of Global IMS Infrasound Data, in: Le Pichon, A., Blanc, E., Hauchecorn, A. (Eds.), Infrasound Monitoring for Atmospheric Studies. Challenges in Middle Atmosphere Dynamics and Societal Benefits. Springer Nature Switzerland AG, pp. 471–482. doi:10.1007/978-3-319-75140-5_13

Christie, D.R., Campus, P., 2010. The IMS Infrasound Network : Design and Establishment of Infrasound Stations, in: Le Pichon, A., Blanc, E., Hauchecorne A. (Eds.), Infrasound Monitoring for Atmospheric Studies. Springer Science+Business Media B.V., 185234-118. doi: 10.1007/978-1-4020-9508-5_2

De Carlo, M., Ardhuin, F., Le Pichon, A., 2020. Atmospheric infrasound generation from ocean waves in finite depth: unified theory and application to radiation patterns. Geophys. J. Int. 221, 569-585. https://doi.org/10.1093/gji/ggaa015

den Ouden, O.F.C., Assink, J.E., Smets, P.M. Shani-Kadmiel, S., Averbuch, G., Evers, L.G., 2020. CLEAN beamforming for the enhanced detection of multiple infrasonic sources. Geophys. J. Int. 221, 305-317. https://doi.org/10.1093/gji/ggaa010

Evers, L. G., 2008. The Inaudible Symphony: on the Detection and Source Identification of Atmospheric Infrasound. Ph.D. thesis, Technische Universiteit Delft, Netherlands, 160 pp. http://resolver.tudelft.nl/uuid:4de38d6f-8f68-4706-bf34-4003d3dff0ce

Garcès, M.A., 2013. On infrasound standards, part 1: Time, frequency, and energy scaling. InfraMatics 2, 13-35. doi: 10.4236/inframatics.2013.22002

Garcès, M., Willis, M., Hetzer, C., Le Pichon , A., Drob, D., 2004. On using ocean swells for continuous infrasonic measurements of winds and temperature in the lower, middle, and upper atmosphere. Geophys. Res. Lett. 31, L19304. doi: 10.1029/2004GL020696

Garcès M., Willis, M., Le Pichon, A., 2010. Infrasonic Observations of Open Ocean Swells in the Pacific: Deciphering the Song of the Sea, in: Le Pichon, A., Blanc, E., Hauchecorne A. (Eds.), Infrasound Monitoring for Atmospheric Studies. Springer Science+Business Media B.V., pp. 235-248. doi: 10.1007/978-1-4020-9508-5_7

Ghica, D, Grecu, B., Popa, M., 2019. Seismo-acoustic observation of the ocean swell sources at BURAR site. Paper presented at CTBT: Science and Technology Conference SnT2019, 24-28 June 2019, Vienna, Austria

Gibbons, S.J., Ringdal, F., Kvaerna, T., 2008. Detection and characterisation of seismic phases using continuous spectral estimation on incoherentand partially coherent arrays. Geophys. J. Int.,172,405–421. https://doi.org/10.1111/j.1365-246X.2007.03650.x

Green, D.N., 2015. the spatial coherence structure of infrasonic waves: analysis of data from International Monitoring System arrays. Geophys. J. Int., 201, 377-389. https://doi.org/10.1093/gji/ggu495

Hasselmann, K., 1963. A statistical analysis of the generation of microseisms. Rev. Geophys. 1(2), 177. doi:10.1029/rg001i002p00177

Hetzer, C.H., Gilbert, K.E., Waxler, R., Talmadge, C.L., 2010. Generation of Microbaroms by Deep-Ocean Hurricanes, in: Le Pichon, A., Blanc, E., Hauchecorne A. (Eds.), Infrasound Monitoring for Atmospheric Studies. Springer Science+Business Media B.V., pp. 249-262. doi: 10.1007/978-1-4020-9508-5_8

Hetzer, C.H., Waxler, R., Gilbert, K.E., Talmadge, C.L., Bass, H.E., 2008. Infrasound from hurricanes: Dependence on the ambient ocean surface wave field. Geophys. Res. Lett. 35, L14609. doi: 10.1029/2008GL034614

Hupe, P., Ceranna, L., Pilger, C., De Carlo, M., Le Pichon, A., Kaifler, B., Rapp, M., 2018. Assessing middle atmosphere weather models using infrasound detections from microbaroms. Geophys. J. Int. 216, 1761–1767. doi:10.1093/gji/ggy520

Husebye, E.S., 1969. Direct measurement of dT/dΔ. B.Seismol.Soc.Am., 59, 717-727.

Landès, M., Ceranna, L., Le Pichon, A., Matoza, R.S., 2012. Localization of microbarom sources using the IMS infrasound network. J. Geophys. Res. 117, D06102. doi: 10.1029/2011JD016684

Landsea, C. W., Franklin, J. L., 2013. Atlantic Hurricane Database Uncertainty and Presentation of a New Database Format. Mon. Wea. Rev. 141, 3576-3592. https://doi.org/10.1175/MWR-D-12-00254.1

Le Pichon, A., Cansi, Y., 2003. PMCC for infrasound data processing. InfraMatics 02, 1-9.

Le Pichon, A., Ceranna, L., Vergoz, J., 2012. Incorporating numerical modeling into estimates of the detection capability of the IMS infrasound network. J. Geophys. Res. 117, D05121. doi: 10.1029/2011JD016670

Le Pichon, A., Vergoz, J., Blanc, E., Guilbert, J., Ceranna, L., Evers, L., Brachet, N., 2009. Assessing the performance of the International Monitoring System's infrasound network: Geographical coverage and temporal variabilities. J. Geophys. Res. 114, D08112. doi: 10.1029/2008JD010907

Longuet-Higgins, M.S., 1950. A theory of the origin of microseisms. Philos. Trans. R. Soc. London 243, 1–35.

Marty, J., 2019. The IMS Infrasound Network: Current Status and Technolofical Developments, in: Le Pichon, A., Blanc, E., Hauchecorn, A. (Eds.), Infrasound Monitoring for Atmospheric Studies. Challenges in Middle Atmosphere Dynamics and Societal Benefits. Springer Nature Switzerland AG, pp. 3–62. doi:10.1007/978-3-319-75140-5_1

Mentaschi, L., Besio, G., Cassola, F., Mazzino, A., 2015. Performance evaluation of Wavewatch III in the Mediterranean Sea. Ocean Model. 90, 82-94. doi: 10.1016/j.ocemod.2015.04.003

Posmentier, E.S., 1967. A theory of microbaroms. Geophys. J. R. astr. Soc. 13, 487-501.

Rascle, N., Ardhuin, F., 2013. A global wave parameter database for geophysical applications. Part 2: Model validation with improved source term parameterization. Ocean Model. 70, 174-188. doi: 10.1016/j.ocemod.2012.12.001

[dataset] Šindelářová, T., Czanik, C., Ghica, D., 2020. Data supporting the research paper Infrasound signature of the post-tropical storm Ophelia at the Central and Eastern European Infrasound Network. 4TU. Centre for Research Data. doi:10.4121/uuid:28bbb57a-cf4e-4dd2-8c21-7a49e27af03b

Šindelářová, T., Kozubek, M., Chum, J., Potužníková, K., 2016. Seasonal and diurnal variability of pressure fluctuation in the infrasound frequency range observed in the Czech microbarograph network. Studia Geophys. Geod. 60, 747-762. doi: 10.1007/s11200-015-0250-1

Stewart, S.R., 2018. Tropical cyclone report. Hurricane Ophelia (AL172017). https://www.nhc.noaa.gov/data/tcr/AL172017_Ophelia.pdf (accessed 29 August 2019).

Stopa, J.E., Cheung, K.F., Garcès, M.A., Badger, N., 2012. Atmospheric infrasound from nonlinear wave interactions during Hurricanes Felicia and Neki of 2009. J. Geophys. Res. 117, C12017. doi: 10.1029/2012JC008257

Stopa, J.E., Cheung, K.F., Garcès, M.A, Fee, D., 2011. Source of microbaroms from tropical cyclone waves. Geophys. Res. Lett. 38, L05602. doi: 10.1029/2010GL046390

Szuberla, C.A.L., Olson, J.V., 2004. Uncertainties associated with parameter estimation in atmospheric infrasound rays. J. Acoust. Soc. Am. 115, 253-258. doi: 10.1121/1.1635407

Tailpied, D., 2016. Évaluation et optimisation de réseau infrason pour la surveillance volcanique (PhD thesis). Institut de Physique du Globe de Paris.

Waxler, R., Gilbert, K.E., 2006. The radiation of atmospheric microbaroms by ocean waves. J. Acoust. Soc. Am. 119, 2651-2664. doi: 10.1121/1.2191607

Willis, M., Garcès , M., Hetzer, C., Businger, S., 2004. Infrasonic observations of open ocean swells in the Pacific: Deciphering the song of the sea. Geophys. Res. Lett. 31, L19303. doi: 10.1029/2004GL020684

Figure captions

Fig. 1. Geography of the CEEIN network (triangles) and Ophelia tracking (after Stewart, 2018). The position of the storm centre in 6-hours intervals is shown from 15 October 2017 00:00 UTC to 17 October 2017 18:00 UTC. On 15 October, Ophelia was a tropical cyclone of hurricane intensity (diamonds). On 16 October by 00:00 UTC, the transition to an extratropical cyclone was completed (circles). Grey squares stand for the approximate location of the reported landfalls.

Fig. 2. Layouts of the CEEIN stations (left column), array responses to a planar wave at 0.1 Hz (middle column), and array responses to a planar wave at 0.6 Hz (right column). Px and Py are the x and y component of the slowness vector. The cyan circle marks the apparent velocity of 340 $m \cdot s^{-1}$ (after Evers, 2008). A colour figure is available online.

Fig. 3. The detections in the microbarom frequency range 0.1-0.6 Hz at the CEEIN stations from 1 to 31 October 2017. The amplitude of the signal is colour coded. The life-time of the Ophelia event is indicated by the green shaded rectangle. Missing data are defined as time intervals longer than 60 s and with data available from less than three sensors; indicated by grey rectangles. The data are smoothed by applying a moving time window of 60-minute length and with 90 % overlap; the error bars represent the standard deviations from the mean back-azimuth. A colour figure is available online.

Fig. 4. Snapshots of the microbarom source from 15 October 2017, 18:00 UTC to 17 October 2017, 18:00 UTC at 6-hour intervals. The geometrical attenuation relative to the barycentre of the CEEIN stations is considered. The triangles represent the CEEIN stations. The station PSZI is close to the barycentre and therefore it is represented by a different marker. The track of Ophelia is shown. The diamonds represent position of Ophelia at the hurricane stage; circles represent position of the post-tropical storm. The arrows represent stratospheric winds at 1hPa (48 km of altitude). A colour figure is available online.

Fig. 5. Comparison of the observations (blue circles online, grey circles in the printed version) with the modelling results for each frequency band (magenta diamods online, black diamonds in the printed version) at CEEIN stations BURARI, PVCI, and PSZI from 15 to 18 October 2017. Left: observed and modelled back-azimuths, the size of the diamonds codes the

corresponding amplitude in the respective frequency bands; right: observed and modelled signal amplitudes. The amplitudes are normalized by their mean background value before and after the event. The units of the normalized amplitudes are dimensionless. A colour figure is available online.

Supplementary figures

S.1. Detail of detections in the microbarom frequency range 0.1-0.6 Hz at PVCI from 15 to 18 October 2017. Data are unsmoothed.

S.2. Detail of detections in the microbarom frequency range 0.1-0.6 Hz at WBCI from 15 to 18 October 2017. Data are unsmoothed.

S.3. Detail of detections in the microbarom frequency range 0.1-0.6 Hz at PSZI from 15 to 18 October 2017. Data are unsmoothed. The grey rectangle indicates time interval with missing data.

S.4. Detail of detections in the microbarom frequency range 0.1-0.6 Hz at BURARI from 15 to 18 October 2017. Data are unsmoothed.

S.5. Detail of detections in the microbarom frequency range 0.1-0.6 Hz at IPLOR from 15 to 18 October 2017. Data are unsmoothed.

S.6. Snapshots of the microbarom source from 15 October 2017, 03:00 UTC to 18 October 2017, 00:00 UTC at 3-hour intervals. The geometrical attenuation relative to the barycentre of the CEEIN stations is considered. The triangles represent the CEEIN stations. The station PSZI is close to the barycentre and therefore it is represented by a different marker. The track of Ophelia is shown. The diamonds represent position of Ophelia at the hurricane stage; circles represent position of the post-tropical storm. The arrows represent stratospheric winds at 1hPa (48 km of altitude).

Tables

Stations	PVCI	WBCI	PSZI	BURARI	IPLOR
Location	Central Czechia	Western Czechia	Northern Hungary	Northern Romania	Central Romania
Latitude Longitude	50.53°N 14.57°E	50.25°N 12.44°E	47.92°N 19.89°E	47.62°N 25.22°E	45.85°N 26.65°E
Nb of sensors	3	4	4	4	6
Type of sensor	The Scientific and Technical Centre "Geophysical Measurements" ISGM03	Paroscientific 6000-16B-IS	SeismoWave MB3d	Chaparral Physics Model 21	Chaparral Physics Model 25
Array aperture	200 m	4-10km	250m	1200m	2400m
Array bandwidth	0.14-3.4 Hz	0.0028-0.068 Hz	0.11-2.72 Hz	0.02-0.57 Hz	0.01-0.28 Hz
Date of installation	2014/05/01	2016/09/28	2017/05/25	2016/07/27	2009/05-2012/08

Table 1. Main characteristics of the CEEIN arrays. The array bandwidths were estimated according to Garcès (2013).

Stations	PVCI	WBCI	PSZI	BURARI	IPLOR
Detection range	0.05-4 Hz	0.0033-0.4 Hz	0.09-7.1 Hz	0.09-7.08 Hz	0.09-7.08 Hz
Window length	60-10 s	2555-118 s	60-12.35 s	410-17s	253-23 s
Window overlap	90 %	90 %	95 %	95 %	95 %
Consistency	0.1 s	3 s	0.2 s	0.2 s	0.2 s
Filter	Chebyshev	Chebyshev	Chebyshev	Chebyshev	Chebyshev
Azimuth tolerance for families forming	10°	3°	3°	3°	3°
Family size	10-50 pixels	15-50 pixels	100-2000 pixels	40-2000 pixels	40-2000 pixels

Table 2. Main parameters of PMCC configurations.

	Ophelia position		PVCI		WBCI		PSZI		BURARI		IPLOR	
UTC	Latitude [°N]	Longitude [°E]	Azimuth [°]	Distance [km]	Azimuth [°]	Distance [km]	Azimuth [°]	Distance [km]	Azimuth [°]	Distance [km]	Azimuth [°]	Distance [km]
2017/10/15 18:00	43.1	-14.3	260	2329	259	2175	271	2694	275	3094	280	3228
2017/10/16 00:00	47.6	-13.4	272	2051	271	1901	282	2469	284	2865	288	3025
2017/10/16 06:00	50	-12.1	279	1886	279	1742	288	2329	290	2717	293	2891
2017/10/16 12:00	52.3	-10	286	1707	287	1571	294	2170	295	2546	299	2732
2017/10/16 18:00	55.3	-8.3	298	1614	300	1497	304	2094	303	2446	306	2647
2017/10/17 00:00	57.3	-6.1	307	1540	310	1442	311	2023	309	2351	312	2561
2017/10/17 06:00	58.7	-2.9	316	1439	320	1360	317	1915	314	2218	317	2434
2017/10/17 12:00	59.3	1.5	325	1280	330	1224	323	1742	319	2019	321	2239
2017/10/17 18:00	60.1	5.3	335	1213	340	1184	331	1648	325	1891	326	2115

Table 3. Track of the storm Ophelia (Landsea and Franklin, 2013). Distances and back-azimuths of the storm centre from the CEEIN stations are stated.

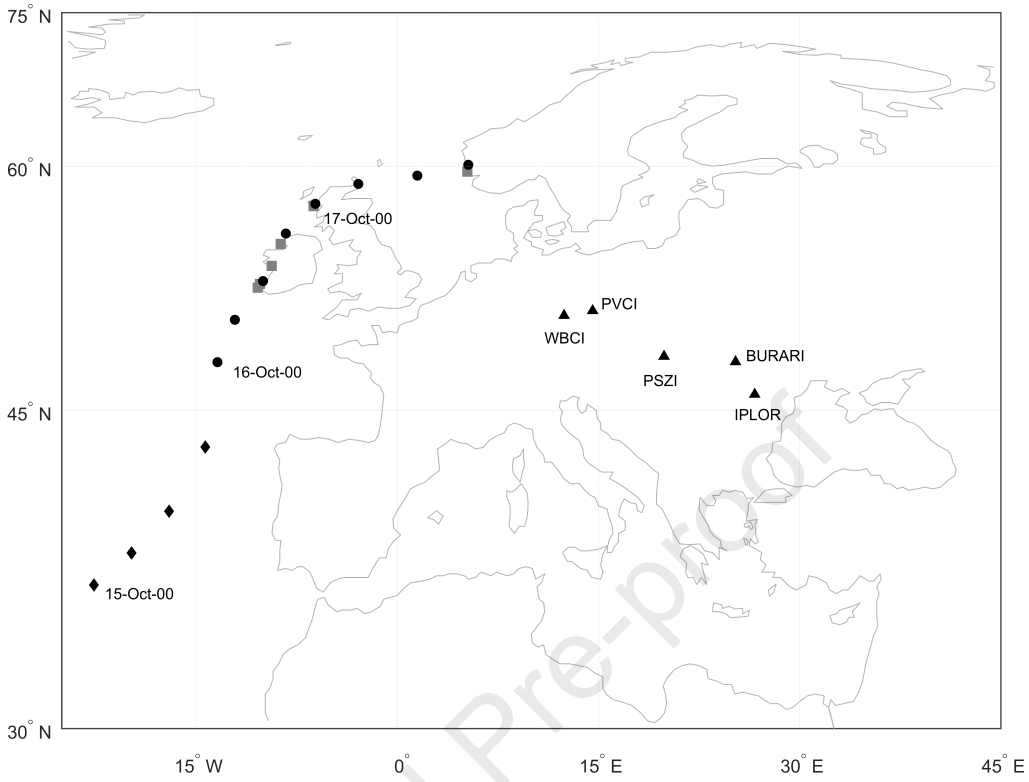

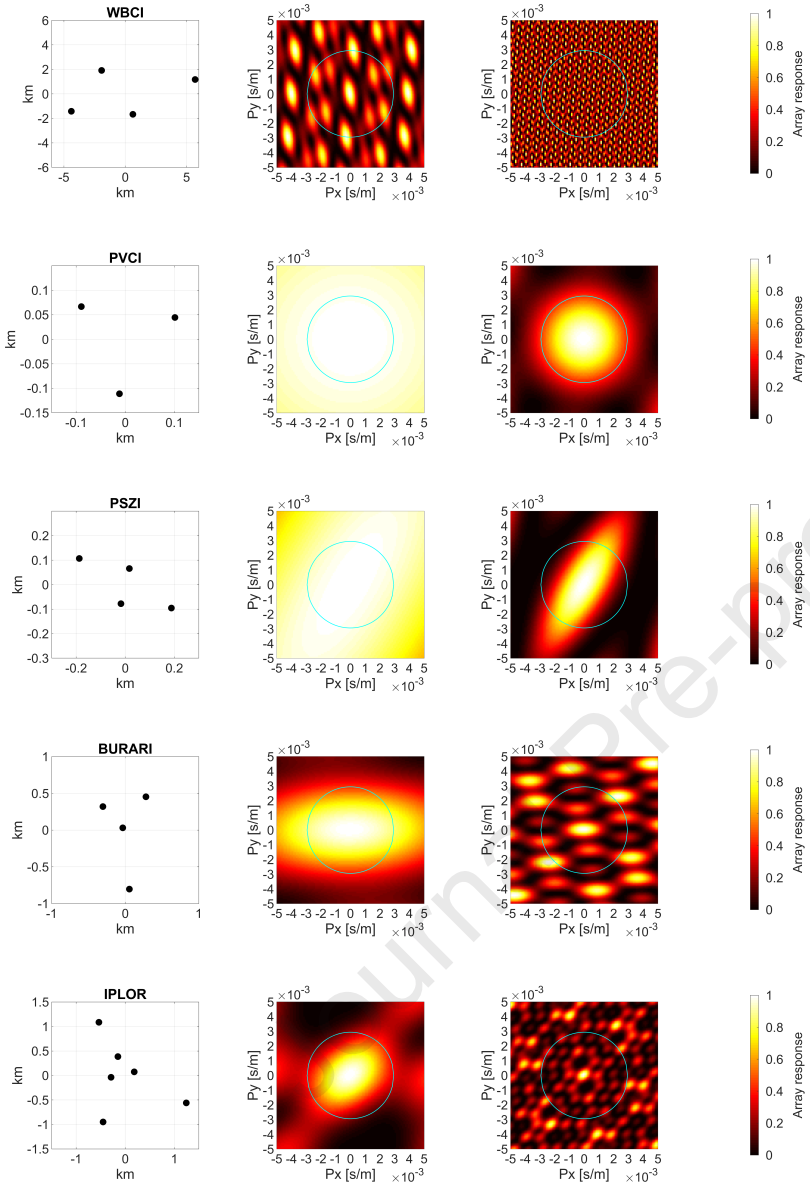

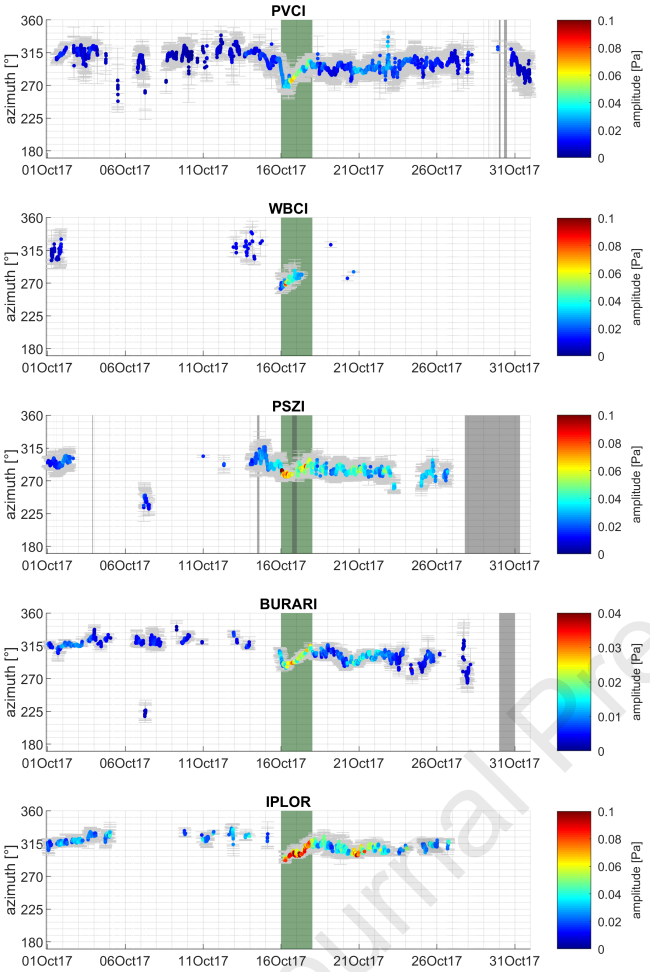

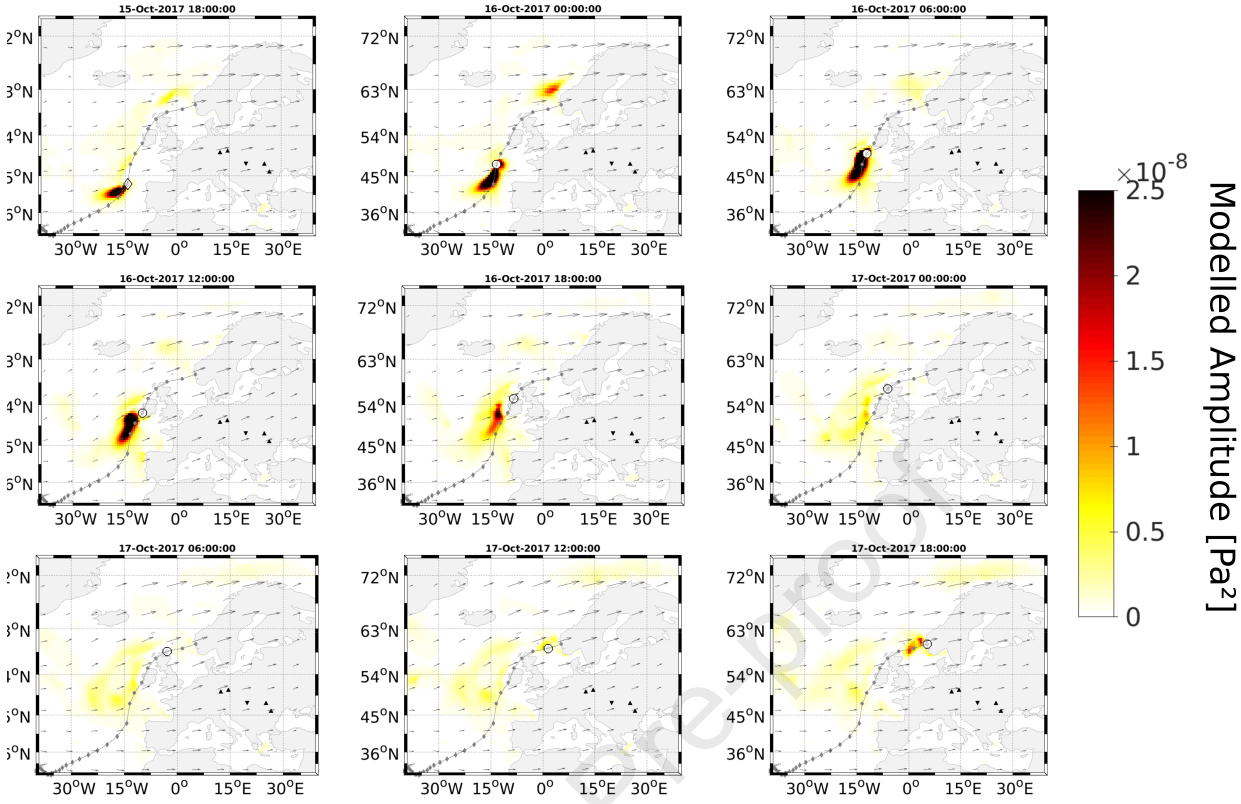

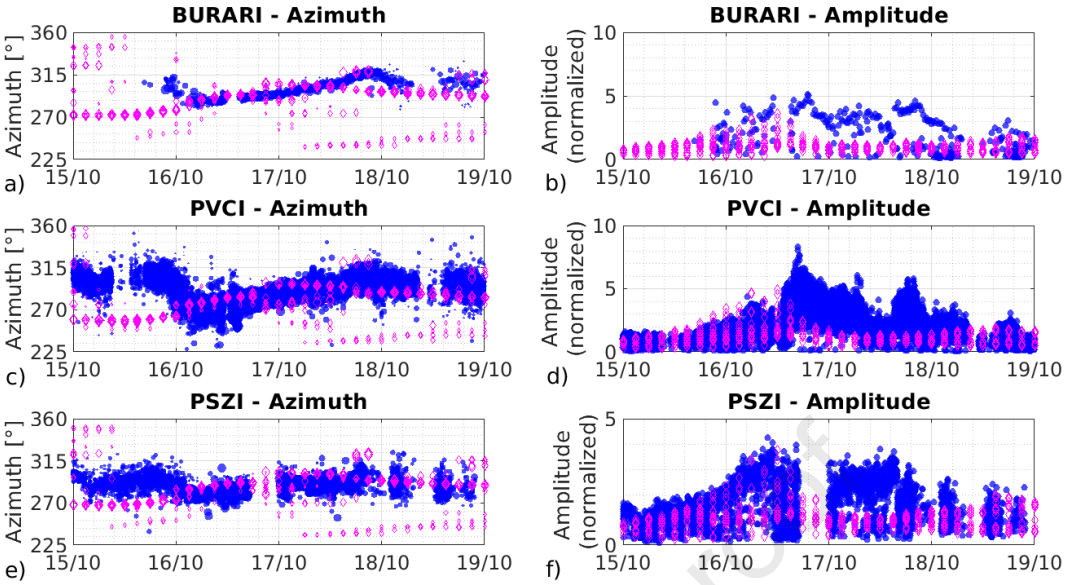

- Unusual microbarom arrivals in central and eastern Europe on 15-18 October 2017
- Back-azimuths were shifted by 20-40° from regular directions
- Increase of signal amplitude was observed at the same time
- Microbarom source and propagation was modelled
- The storm Ophelia generated a moving dominant source of microbaroms

Declaration of interests

☒ The authors declare that they have no known competing financial interests or personal relationships that could have appeared to influence the work reported in this paper.

☐The authors declare the following financial interests/personal relationships which may be considered as potential competing interests: